ELSEVIER

Polymer 43 (2002) 4905–4913

polymer

www.elsevier.com/locate/polymer

Isothermal crystallization kinetics of nylon 6, blends and copolymers using simultaneous small and wide-angle X-ray measurements

N.S. Murthy[a,*], Z.-G. Wang[b], M.K. Akkapeddi[a], B.S. Hsiao[b,**]

[a]*Specialty Materials, Honeywell International Inc., Morristown, NJ 07962, USA*
[b]*Department of Chemistry, State University of New York at Stony Brook, Stony Brook, NY 11794-3400, USA*

Received 30 April 2002; accepted 2 May 2002

Abstract

Crystallization behavior in a number of blends and copolymers of nylons (polyamides) was investigated using time-resolved X-ray scattering data obtained simultaneously in the small- and wide-angle regimes. The following samples studied were: nylon 6 homopolymers (N6) of different molecular weights, copolymers of N6 and nylon 6,6 (N6/66), and blends of these with an amorphous nylon (N6I/T), which is a 70:30 random copolymer of poly(hexamethylene isophthalamide) and poly(hexamethylene terephthalamide). Addition of comonomers and blending with the N6I/T reduces the crystallinity of N6. Isothermal crystallization data obtained at several temperatures showed the expected faster crystallization kinetics at higher degrees of supercooling. Comonomer units in the N6 backbone reduce the rate of crystallization. N6I/T affects the crystallization (lamellar growth) behavior of N6/N66: the rate is higher at temperatures above the T_g of N6I/T (120 °C) where the crystallization is nucleation-driven, and lower below the T_g of N6I/T where it is growth-driven. Lamellar spacing decreases with an increase in the degree of supercooling, and this decrease is smaller in the blends than in the homopolymer. Larger lamellar spacing in N6I/T blends is due not to the insertion of N6I/T segments into the interlamellar regions but to an increase in the lamellar thickness. Blending seems to change the morphology by affecting the crystallization behavior rather than by thermodynamic phase separation. Residual monomers, which act as plasticizers, dramatically reduce the crystallization rate, whereas shear or similar mechanical history of the resin considerably accelerate the crystallization rate.

Keywords: Nylon 6; Crystallization kinetics; Small and wide-angle X-ray analysis

1. Introduction

Nylons, or aliphatic polyamides, are widely used in many applications as homopolymers, copolymers and blends. Despite numerous studies on the synthesis and properties of these polymers [1,2], there are only a few reports on the fundamental behavior related to the crystallization behavior at the lamellar level [3,4], and only one using time-resolved X-ray diffraction/scattering methods to probe the structure and morphology development simultaneously [5]. A study of the crystallization behavior, and how this changes in polymers with different formulations, thermal history, and additives are not just of academic interest but of immense practical value. Such data are necessary to calculate the optimal molding parameters, e.g. time–temperature profiles during injection molding, for the various grades or types of nylons, and for parts of various thickness and geometry.

In this paper we present our simultaneously obtained small-angle X-ray scattering (SAXS) and wide-angle X-ray diffraction (WAXD) data as a part of our program to develop database and to predict the polymer properties. We study nylon 6 (N6), random copolymers of N6 and nylon 6,6 (N6,6) that is identified as N6/66, and blends of N6/66 with an amorphous aromatic nylon N6I/T, a random copolymer (70:30) of poly(hexamethylene isophthalamide), 6I, and poly(hexamethylene terephthalamide), 6T. We report the crystallization kinetics of these polymers and analyze the effect of the comonomer (N66) and blend components (amorphous nylon, N6I/T). We also analyze the effects of end groups, molecular weight and processing history on the crystallization kinetics as well as the change in the lamellar development.

2. Experimental

N6 homopolymer, and copolymers of N6 and N6,6

* Corresponding author. Tel.: +1-516-632-7793; fax: +1-516-632-6518.
** Corresponding author. Tel.: +1-973-455-3764; fax: +1-973-455-2936.
E-mail address: murphy@mailaps.org (B.S. Hsiao).
bhsiao@notes.cc.sunysb.edu (B. Chu).

0032-3861/01/$ - see front matter
PII: S0032-3861(02)00307-5

Table 1
Description of the various polyamides used in this work

Polymer composition	Sample ID	FAV	$M_w \times 1000$ g/mol	M_w/M_n	COOH/NH_2 (μmol/g)	T_m (°C)	T_{cc} (°C)	Remelt (°C)	Extractables (wt%)	
									C1	C2–C8
Homopolymers										
Nylon 6	N6-a	45	23	1.9	55/55	222	181		0.37	0.46
Nylon 6	N6-b	64	30	2.1	42/42	222	174		0.12	0.39
Nylon 6	N6-c	60	28	1.8	22/77	222	176		0.41	0.49
Nylon 6	N6-d	158			36/33	222	173		0.15	0.46
Nylon 6	N6-e	158			53/20	222	180		0.26	0.61
Copolymers of nylon 6/6,6										
90/10	90N6-a	120	47			195/198	148	195	4.9	1.09
90/10	90N6-b	140	51			195			4.55	1.12
85/15	85N6-a		31			197/196	156	196	0.19	0.25
85/15	85N6-b					195			6	2
85/15	85N6-c					195			8	2
Blends										
85N6-a + 10% am nylon	10%-N6I/T					196	145	180/189		
85N6-a + 20% am nylon	20%-N6I/T					194	138	179/189		

(N6/66) at ratios of 90:10 (90N6) and 85:15 (85N6) were used in this study. The blends studied were those of the copolymer 85N6 and amorphous nylon (N6I/T; T_g = 120 °C). The samples studied in this report and some of their characteristics are given in Table 1. The five homopolymers of N6 are labeled from N6-a to N6-e. N6-a and N6-b were made from hydrolytic polymerization of caprolactam at 260 °C. Molecular weight was controlled by the reaction time and the water concentration. N6-c was made by a similar non-terminated process as in N6-a and N6-b, but was amine terminated by adding a controlled amount of hexamethylene diamine (HMDA) in the initial monomer mixture. The amount of HMDA determines the molecular weight and the end groups composition. N6-d was a film grade resin that was solid stated at 200–210 °C from N6-b while constantly removing the water of polycondensation. Molecular weight was controlled by the time (typically 12–18 h) spent in the reactor. N6-e had the same M_w as N6-d but was made from N6-b by chain extension in an extruder using an organophosphate as a catalyst for polycondensation. Both 85N6-a and -b were made in a kettle and were similar in composition except that 85N6-a was leached with hot water to remove extractables, and 85N6-b was not leached and hence did not have associated thermal history. 85N6-c had a higher molecular weight than -a and -b (about the same as 90N6-b) as a result of chain-extension in an extruder. 90N6-a and -b were polymerized similar to 85N6-b in a kettle, but 90N6-b had higher M_w than 90N6-a because of longer reaction time. N6I/6T is commercially available as Selar from Du Pont and Grivory 21 from EMS chemie.

The characteristics of the samples listed in Table 1 were determined as follows. Molecular weight distribution of the polymers equivalent to the ones used here was analyzed using gel permeation chromotography (GPC), and the samples used in this study were characterized by relative viscosity in formic acid, usually called the FAV. FAV is the product of the flow time of a 11% polymer solution in 90% formic acid and the viscometer constant. Amine end group was determined by dissolving 2 g of the resin in 50 ml of trifluoroethanol (TFE). The sample was titrated using 0.02N *p*-toluenesulfonic acid in TFE. The end point was detected using a glass pH electrode. Carboxyl end group was determined by dissolving 2 g of the resin in 50 ml of benzyl alcohol. It was necessary to reflux the benzyl alcohol for about 30 min under a nitrogen blanket to completely dissolve the nylon. The benzyl alcohol solution was titrated while still warm using 0.02N sodium hydroxide in benzyl alcohol. The end point was detected using a glass pH electrode. Solvent blanks were also analyzed in both instances. The melting point (T_m) and the crystallization temperature during cooling from the melt (T_{cc}) obtained at 10 °C/min were determined from a DSC scan. Extractables listed in Table 1 are the monomers (C1) and oligomers (C2–C8) that were extracted with water at 115 °C and 1500 psi

and analyzed using high performance liquid chromotography (HPLC).

Simultaneous SAXS and WAXD data were collected by first taking the polymer to a temperature above the equilibrium melting temperature (T_m^0, 260 °C) and quenching the melt to the desired crystallization temperature. The data were obtained on the beam line X27C at the National Synchrotron Light Source, Brookhaven National Laboratory. The wavelength (λ) was 1.307 Å. Both the SAXS and WAXD data were collected using two separate linear position sensitive detectors (EMBL). All the scans were corrected for the background scattering and normalized for the beam fluctuations. The measurements were carried out over several sessions under slightly different instrumental configurations. Typically, the sample-to-detector distance was 220 mm for WAXD and 1560 mm for SAXS; the evolution of the SAXS and WAXD traces as a function of time was monitored by storing the frames every 10 s during the initial stages and 60 s during the final stages.

SAXS data were analyzed using correlation and interface distribution functions as described in detail for N6,6 in our earlier paper [6], and was based on the work of Strobl and Schneider [7]. Briefly, it is assumed that the scattering is due to alternating layers of crystalline lamellae and interlamellar amorphous regions, a two-phase model. The long-spacing L, the distance between the lamellae is given by the position of the first maximum in the correlation function. One of the thicknesses (l_1) of the two phases is determined by modeling the portion of the correlation function before the first minimum [8–10]. The second thickness (l_2) is $L - l_1$. On the basis of other data such as WAXD, DSC and TEM, we have been able to assign the larger of the l_1 and l_2 values to be the crystalline or lamellar thickness (l_c). The linear crystallinity calculated on the basis of l_1 and l_2 ($100l_c/L$) represents the crystallinity of the lamellar stack. Typically this is 60–80% and is much higher than the bulk crystallinity (15–30%) because a significant fraction of the amorphous segments lie outside the lamellar stacks [11, 12]. The bulk crystallinity is determined by comparing the area under the crystalline peak in the WAXD scans to the total scattered intensity [13].

SANS data on the copolymers which were collected at NIST on the 30 m beamline using a λ of 5 Å and a sample-to-detector distance of 13.18 m. The intensities were scaled to absolute values using a water standard. Background obtained from an empty sample holder was subtracted. Radial intensity scans were generated by circular averaging of the 2D data.

3. Results and discussion

Fig. 1 shows an example of the time-resolved simultaneous SAXS and WAXD profiles during isothermal crystallization. Such plots show that, as in many other polymers, the SAXS lamellar peak appear after some induction time, and slightly before the wide-angle crystalline peaks. While the slow-cooled N6 crystallizes into the α form, the crystallinity in the isothermally crystallized samples of the homopolymers (as well as copolymers and blends discussed in later sections) is mostly due to the γ form of nylon and poorly defined/crystallized α form as seen in Fig. 1(b). Thus, the quenching conditions appear to dictate the final crystalline form.

For quantitatively characterizing the development of morphological parameters in these samples, SAXS data were analyzed using the correlation function method to monitor the changes in the invariant (Q), the long period (L) of the lamellar stacks, the lamellar (crystal) thickness (l_c) and the amorphous layer thickness (l_a). The WAXD data were analyzed to follow the increase in the mass degree of crystallinity (X_{mc}, commonly referred to as crystallinity) with time. The details about these methods can be found in previous papers [8–10].

Fig. 2 shows an example of the time evolution of SAXS parameters corresponding to the sample used for Fig. 1. The parameters we measured to characterize the crystallization kinetics are the time t_{c1} for the onset of crystallization (induction time), time t_{c2} for the completion of primary crystallization from the invariant plots, and the final long-spacing. The values of t_{c1} and t_{c2} are large enough to be

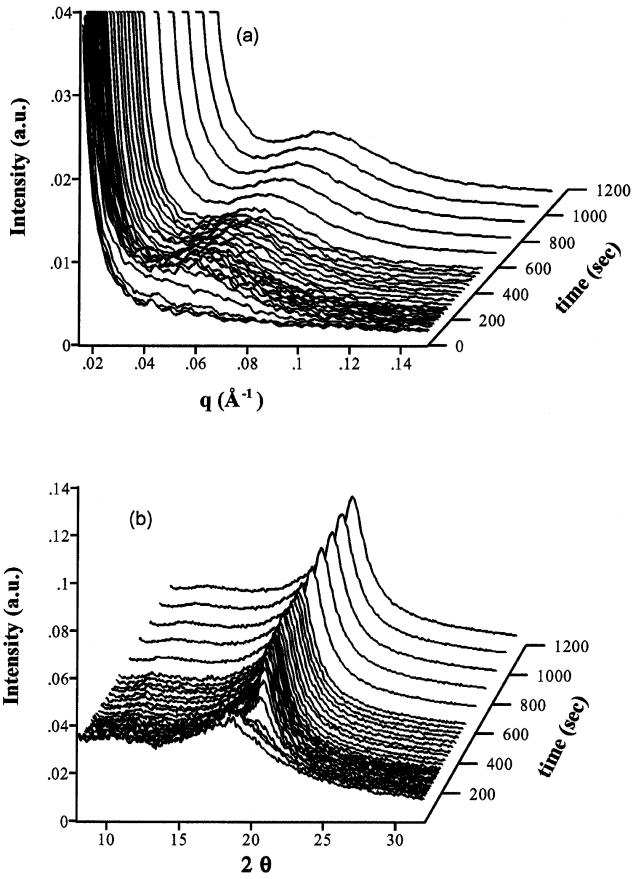

Fig. 1. Example of the time resolved data during isothermal crystallization of 85N6-a (85:15 of N6 and N6,6) at 130 °C. (a) SAXS (b) WAXD.

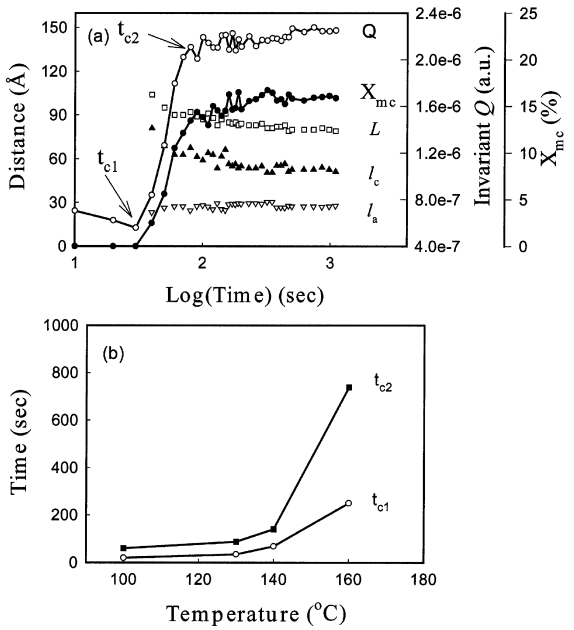

Fig. 2. Evolution of the structural parameters in 85N6-a during isothermal crystallization at 130 °C. (a) Lamellar structure as shown by lamellar spacing L, crystal thickness l_c, the amorphous layer thickness, $l_a = L - l_c$, and the invariant Q. Also shown in the crystallinity as determined from the WAXD data. Data obtained at 130 °C. (b) An example of the variation in the two times t_{c1} and t_{c2} with crystallization temperature.

easily measured, and is shown in Fig. 2(b) for the 85:15 copolymer of N6/N66. The increase in the invariant Q and the crystallinity (X_{mc}) are in good agreement. The degree of crystallinity in these samples is relatively low (<20%) and increases slowly after the primary crystallization stage. Also, the values of L and $l_c (= l_1)$ decrease rapidly during the primary crystallization stage (defined as the stage before the time t_{c2}), and then decrease slowly during the secondary crystallization stage (after the time t_{c2}). In contrast, the amorphous layer thickness ($l_a = l_2$) shows little variation. This phenomenon can be easily explained by the lamellar stack insertion (dual lamellar stacks) model, which can be found in our series of papers on the various semicrystalline polymers such as poly(ether ether ketone), poly(butylene terephthalate), poly(ethylene terephthalate) and N6,6 [14–17].

3.1. Homopolymers

The intent of studying the five homopolymers was to understand what effect, if any, the variables such as molecular weight, end groups and processing history have on the crystallization kinetics of nylon. The five N6 resins studied here identified as N6-a, -b, -c, -d and -e, have different molecular weights, end-groups and processing history as indicated in Table 1. Fig. 3(a) shows the variation in the final long-spacing (L) as a function of degree of supercooling for the various commercial grades of N6 homopolymers. Fig. 3(b) and (c) show the separation of this long-spacing into its two components, the crystal thickness

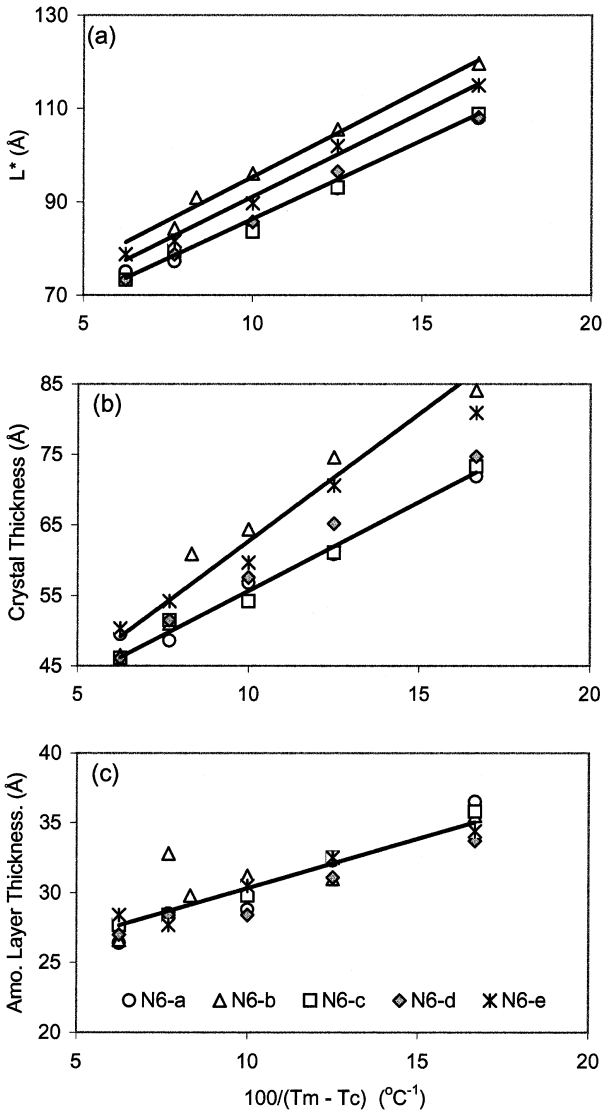

Fig. 3. Plot of (a) lamellar spacing, (b) crystal thickness, and (c) amorphous layer thickness, as a function of crystallization temperature according to Eq. (1).

and the amorphous layer thickness, respectively [14–17]. Only the changes in the crystal thickness with crystallization temperature are accessible to thermodynamic analysis. A simple crystallization theory predicts a straight line for the plot of initial thickness of the chain folded lamellae, l_c^*, as a function of degree of supercooling according to Eq. (1) [18].

$$l_c^* = \Delta l + c/(T_m - T_c) \quad (1)$$

where T_m and T_c are melting and the crystallization temperatures, respectively, and c is a constant. This is what we indeed see in Fig. 3(b), but only when we use 260 °C for the melting point. The generally accepted value for the equilibrium melting point of N6 is in fact 260 °C [19]. The changes in l_c (as well as L) as a function of supercooling in N6-b and N6-e is different from the other three resins. We do not understand why N6-b and N6-e are different from the rest on the basis of the known

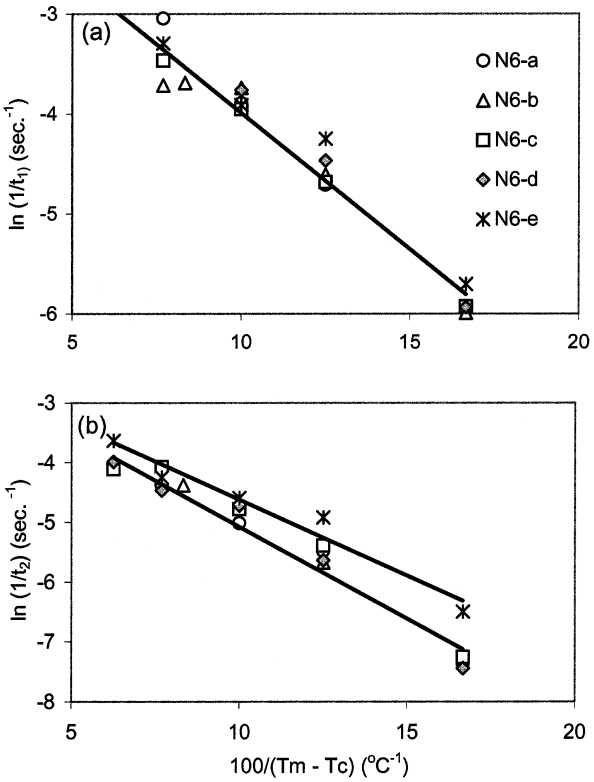

Fig. 4. Dependence of the growth rate with crystallization temperature according to Eq. (2). (a) Induction time t_{c1} and (b) time to complete crystallization t_{c2}.

characteristics of the resins (Table 1) such as the molecular weight (also the equivalent and more commonly used parameter FAV, the relative viscosity in formic acid), end-group compositions and the extractables.

Fig. 4 shows the variation in the induction time (t_{c1}) and time to reach the plateau (t_{c2}) as a function of the degree of supercooling for three resins with different molecular weights, a fourth with a different end-group termination, and a fifth with a very different process history. Magill reported half times ranging from 10 s at 150 °C to 500 s at 200 °C [4]. These are comparable to the time for full crystallization ($t_{c2} - t_{c1}$) values of 60 and 1200 s that we measured using the SAXS invariant at these same temperatures. These plots are used only to compare the differences in the crystallization time of the various resins and not to obtain any thermodynamic parameter. The empirical expression used for the plots is

$$1/\tau = \exp(-K/\Delta T) \quad (2)$$

where τ is either t_{c2} or t_{c1}, K is a constant and ΔT is the degree of supercooling ($T_m^0 - T_c$), and is modeled after the expression for crystal growth as described by Lauritzen and Hoffman [20]. A plot of $\ln(1/\tau)$ vs. $1/\Delta T$ is expected to be a straight line, as seen in Fig. 4. For the polar polymers, the end groups and the molecular weight do not appear to play a significant role. The one resin that has very different behavior (N6-e) illustrates the effect of the additional processing step that involves shear during extrusion. The high molecular weight N6-e resin (150 FAV) was made from a lower (100 FAV) molecular weight resin by solid state polymerization. As a result of the high shear rate that this polymer experiences in the extruder, the polymer retains some residual order even in the melt. These ordered domains act as nucleation sites that accelerate the rate of crystallization in this resin, i.e. reduces t_{c2}. Thus, shear history cannot be erased in the melt.

In addition to isothermal crystallization studies, it is common to measure the temperature of crystallization during cooling (T_{cc}) from the melt at a constant rate (typically at 10 °C/min). Fig. 5 shows a plot of t_{c2} (time to complete crystallization) as a function of T_{cc}. The expectation that higher T_{cc} implies faster crystallization was found to be valid only when crystallization occurs above 180 °C (small degree of undercooling; e.g. $\Delta T = 60$ and 80 °C), and not when crystallization occurs rapidly as the polymer is quenched from the melt to temperatures below 180 °C, i.e. $\Delta T > 80$ °C.

3.2. Copolymers

We studied N6/N66 random copolymers with compositions of 90:10 (samples 90N6-a and -b) and 85:15 (85N6-a, -b and -c). One variable in this group is obviously the comonomer content. In addition, 85N6-b has significant amount of extractables compared to -a–c and -c has a higher molecular weight than -a or -b as a result of chain-extension in an extruder. Fig. 6 shows the changes in the invariant with time for the homopolymer and two of the copolymers. The large increase in times t_{c1} and t_{c2} at 10% copolymer seen in this plot was found to be due to the higher amount of residual monomer content in this particular resin (Table 1). Monomers are known to act as plasticizers and this decreases the rate of crystallization. These times, t_{c1} and t_{c2}, are plotted in Fig. 7. Both t_{c1} and t_{c2} are higher in the presence of the comonomer. The increase in time for complete crystallization (t_{c2}) is also reflected in the larger long-spacing in the sample with the plasticizer (Fig. 7(b)).

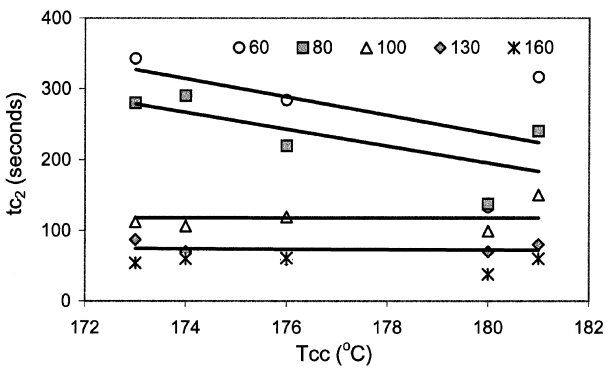

Fig. 5. Correlation between the time for completion of crystallization under isothermal conditions (T_c) and temperature of crystallization upon cooling (T_{cc}) at the various undercoolings ($T_m^0 - T_c$) as indicated in the figure. The times at 60° supercooling is reduced by a factor of 5 for plotting purposes.

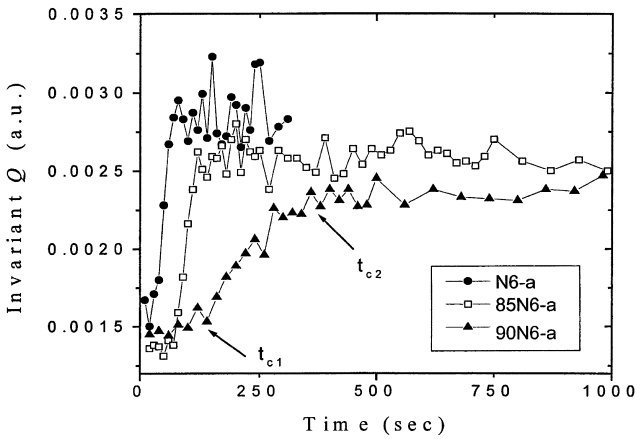

Fig. 6. Comparison of the evolution of the lamellar structures in homopolymers and two copolymers, as indicated by the changes in the invariant at 140 °C.

Fig. 8 shows the variation in the long-spacing, crystal thickness and the amorphous layer thickness with crystallization temperature ($T_m^0 = 225$ °C; unpublished results). As with homopolymers, the long-spacing increases with the temperature of crystallization. This increase in the lamellar spacing is mostly due to an increase in the crystal thickness; the high chain mobility at high temperature favors disentanglement and rearrangement of the chains, resulting in the thicker lamellae. Similarity between the behavior of the homopolymer and the copolymer indicates the minimal disruption in the crystal growth characteristics due to the presence of the comonomer.

The differences in the crystallization rates with the degree of supercooling among the various copolymers are

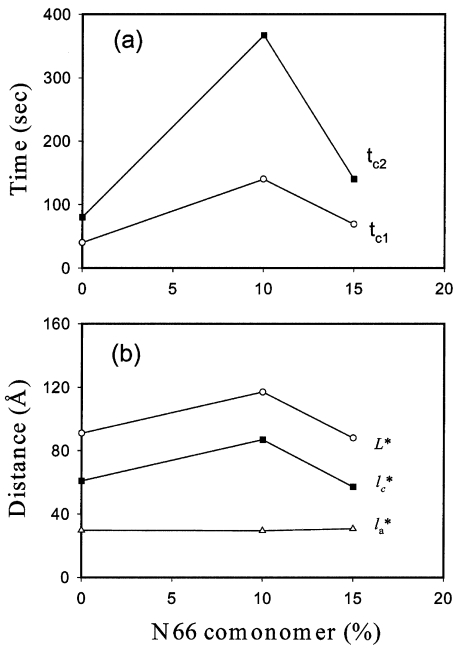

Fig. 7. Effects of the comonomers on (a) the kinetics, i.e. crystallization times, and (b) the structural parameters, i.e. L, l_c and l_a of the copolymer. The data were obtained at 140 °C.

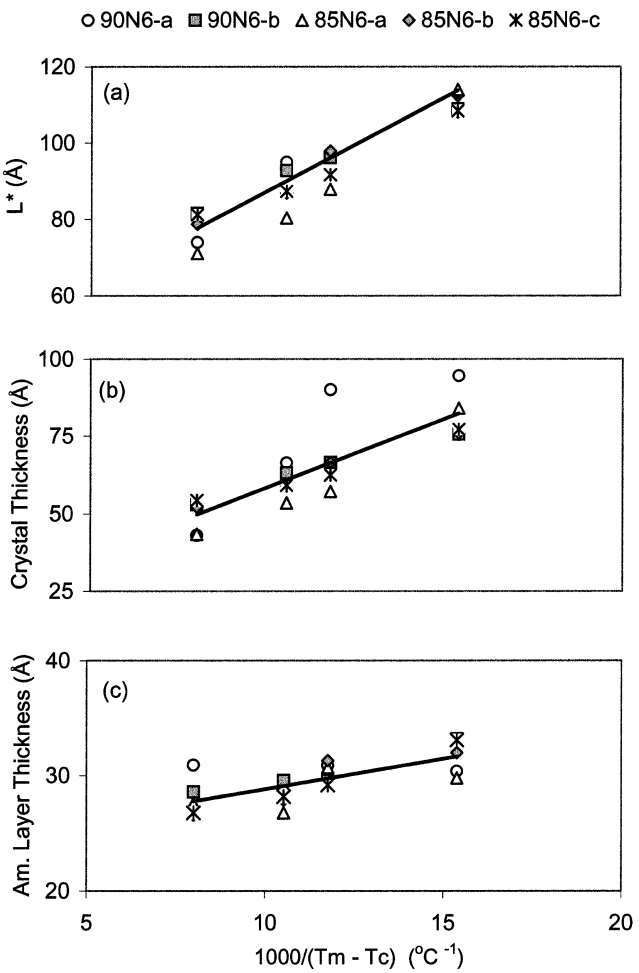

Fig. 8. Comparison of the lamellar spacing variations with crystallization temperature in homopolymers and copolymers.

compared with that of a homopolymer in Fig. 9 in the form of a $\ln(1/\tau)$ vs. $1/\Delta T$ plot (τ is induction time t_{c1} or time to reach the plateau t_{c2}). Again, as with homopolymers, the resin with shear history (85N6-c) crystallizes faster than other resins. Also note that although copolymers crystallize at a lower temperature, when plotted as a function of degree of undercooling, the rate of crystallization in copolymers is faster than that in homopolymers. This could be because the N66 segments crystallize earlier than N6 at a given temperature, thereby increasing nucleation and the rate of crystallization of N6 in the copolymer over the N6 homopolymer. WAXD data show that the crystals are more disordered in copolymer than in homopolymers.

Neutron scattering measurements were carried out on a random copolymer N6 and N66 by deuterating one of the components to study the distribution of the two components in the bulk of the sample. SANS data from the as synthesized and annealed 50:50 deuterated N6/normal N6,6 (not in Table 1) are shown in the form of a Porod plot in Fig. 10. The polymer melts at 195 °C, crystallizes from the melt during cooling (rate: 10 °C/min) at 151 °C, and remelts at 182 and 192 °C upon reheating. The double

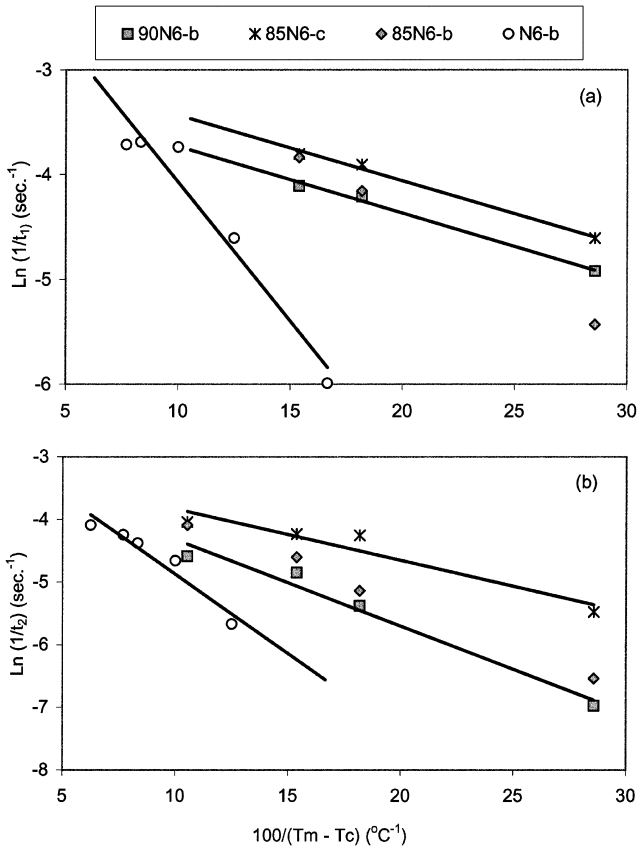

Fig. 9. Dependence of the growth rate with crystallization temperature according to Eq. (2) for copolymers: (a) induction time t_{c1} and (b) time to complete crystallization t_{c2}.

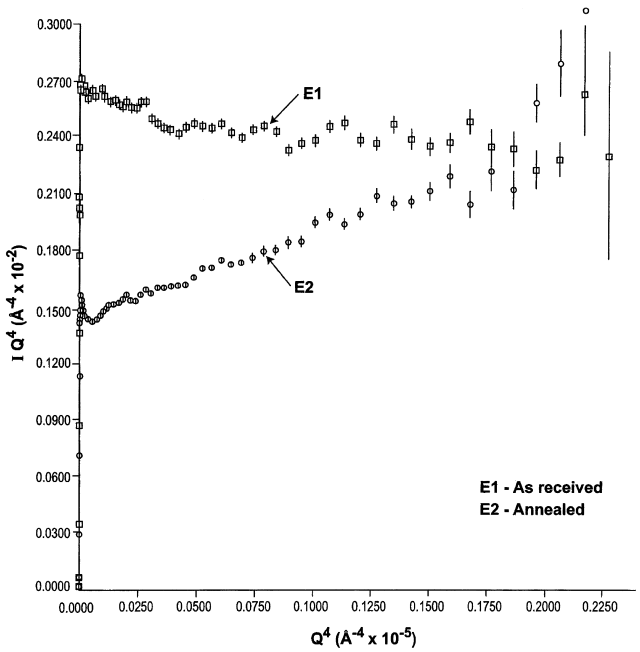

Fig. 10. SANS data from (a) as synthesized and (b) annealed N6/66 copolymer.

melting peaks upon reheating are typical for many polymers, especially nylons. These values suggest the composition of 6:6,6 ratio in the copolymer to be about 75:25 [21]. Relative viscosity was 0.82 compared to 1.35 in the commercial 85:15 N6:6,6 copolymer and 1.35 in the equivalent N6 resin. The positive slope in the annealed sample shows that large-scale inhomogeneities occur upon annealing. However, DSC scans of the annealed specimens were almost identical to that of the as-polymerized material, the only difference being that the crystallization temperature upon cooling from the melt was 153 instead of 151 °C. If the comonomers are incorporated into the lamellae for kinetic reasons, then after annealing or crystallization, there would be a marked difference in the distribution of the comonomers in the crystalline and amorphous regions, and this would be evident in the change in the melting and recrystallization behavior. Absence of such a melting point difference is consistent with the formation of eutectic crystals in which one comonomer (N6,6) is not expected to be included in the crystals of the other comonomer (N6).

The SANS data for the as-received sample suggest that even though N66 segments are excluded from the N6 crystals, the N66 segments are uniformly distributed in the amorphous N6 matrix both between the lamellae and outside the lamellae in the as-polymerized sample. But, inhomogeneities do occur upon annealing as seen by the positive slope in the Porod plot. These inhomogeneities are large-scale segregation of deuterated N6 and non-deuterated N6,6 in the amorphous regions resulting from the enhancement of N6 in the interlamellar regions. Thus, phase separation of the N6- and N66-rich segments could occur in the amorphous phase, between two amorphous domains, one between the lamellae and the other outside the lamellar stacks, without affecting the melting and crystallization behavior of the N6 crystals.

3.3. Blends

It has been shown that amorphous aromatic and aliphatic nylons are miscible [22–26]. However, there have been reports of heterogeneities in these blend systems that are likely due to the crystallization process. Here, we address this issue by studying the kinetics of crystallization of the crystallizable polymer (N6) in the presence of non-crystallizable polymer (N6I/T). Fig. 11 shows the changes in the crystallization time with blends of a 85:15 copolymer (85N6) with 10 and 20% amorphous nylon; the samples are labeled 10 and 20%-N6I/T, respectively. N6I/T stands for the (70:30) random copolymer of poly(hexamethylene isophthalamide), 6I, and poly(hexamethylene terephthalamide), 6T. These miscible blends have a composition dependent T_g [27], and the data in Fig. 11 show the effect of varying $T_c - T_g$. The crystallization temperatures upon cooling from the melt at 10 °C/min for 85N6, 10 and 20%-N6I/T are 156, 145 and 138 °C, respectively. This shows that blending with amorphous nylon retards the

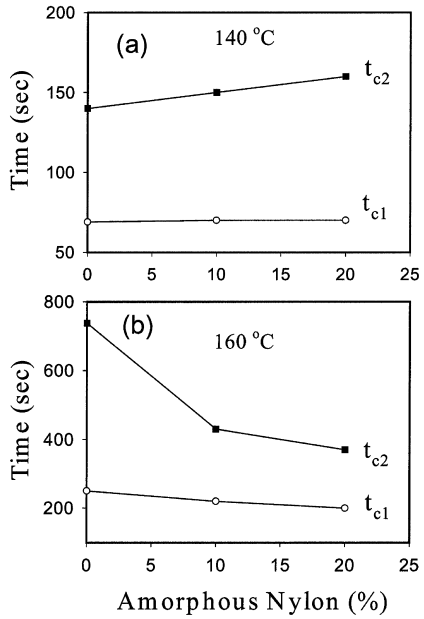

Fig. 11. Variation in the crystallization times at two crystallization temperatures in N6/66 blended with amorphous nylon.

crystallization behavior of the copolymer 85N6 at low crystallization temperatures (e.g. 140 °C). But at higher temperatures (e.g. 160 °C), it accelerates the crystallization. Such changes in the crystallization rates can account for the differences in the crystallinities of the blend and the homopolymer [27].

The changes in the crystallization rates can be understood in terms of the two processes, nucleation and growth, that determine the crystallization rates. The Turnbull–Fischer expression for growth rate is [28]

$$\ln G = \ln G_0 - (\Delta E^*/kT_c) - (\Delta F^*/kT_c) \quad (3)$$

where G is the spherulite growth rate, G_0 a pre-exponential factor, k the Boltzmann constant, T_c the crystallization temperature, ΔE^* the free energy of activation for transporting a chain segment from the melt to the crystalline phase, and ΔF^* is the free energy of formation of nucleus of critical size. At high temperatures, when T_c approaches T_m, the nucleation term $(-\Delta F^*/kT_c)$ determines the crystallization rate. It could be that in the presence of non-crystallizable amorphous nylon segregation of the crystallizable nylon in the melt is promoted. This local ordering will aid the conformational rearrangements of the crystallizable segments and enhance the rate of formation of crystallites. At low temperatures, when T_c is far below T_m, the transportation term $(-\Delta E^*/kT_c)$ is the overwhelming factor, and the mobility of the polymer determines the crystallization rate. Amorphous nylon, whose T_g is about 120 °C, probably impedes the diffusion of N6 chains and thus increase the time to full crystallization. Increase in the lamellar thickness and the long period (Fig. 12) could be a consequence of the increase in the time to complete the crystallization process.

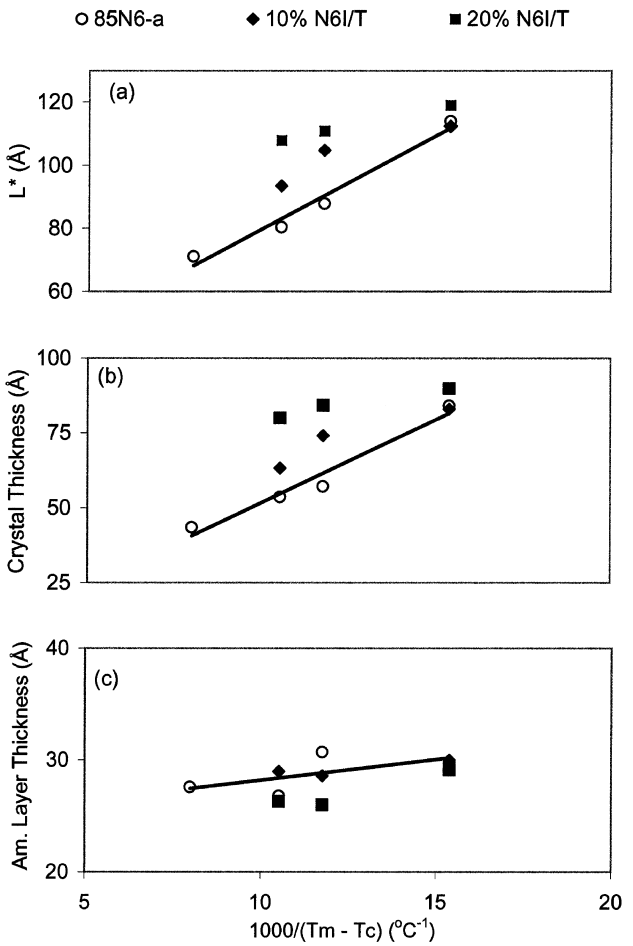

Fig. 12. Variation in the long-spacing as a function of degree of supercooling in nylon blends.

Fig. 12 shows the changes in the long-spacing in blends and the starting polymer at various crystallization temperatures. The lamellar repeat in blends is larger than the host polymer at large degrees of undercooling (lower crystallization temperatures), and this difference disappears at small degree of undercoolings (higher crystallization temperatures). At first glance this increase in the lamellar spacing appears to be due to insertion of the amorphous nylon into interlamellar spaces. However, the data show that the amorphous layer thickness does not change with the addition of the amorphous nylon. This is consistent with the results of Myers et al. [27]. While the amorphous phase between the lamellae within the lamellar stacks is depleted of the amorphous nylon segments, the amorphous nylon expelled into the space outside the lamellar stacks forms a homogeneous single phase with the amorphous N6/66 segments. We find that the increase in the lamellar spacing is in fact due to the increase in the thickness of the lamellae. The increase in the thickness of the lamellae is consistent with the lower T_{cc} in the presence of amorphous nylon. The crystallinity decreases with the increase of amorphous content in the blends, a behavior similar to that seen with increase in comonomer content (Fig. 13). Also, the

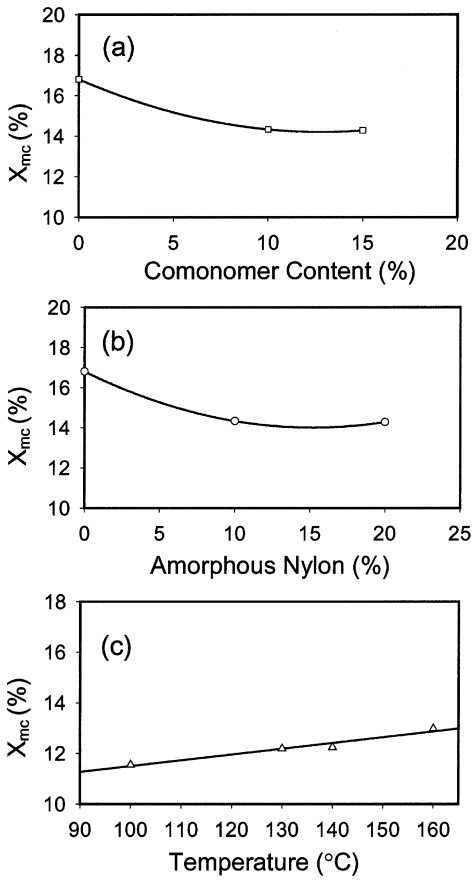

Fig. 13. Variation in apparent crystallinity with (a) comonomer content in the copolymer, (b) amorphous nylon content in the blend, both at a crystallization temperature of 130 °C, and (c) with temperature of crystallization for 85N6 with 10% amorphous nylon.

crystallinity increases slightly with crystallization temperature (Fig. 13(c); 85N6 blends with 10% am.nylon). Our results in essence show that, as speculated by Myers et al. [27], the features that we see in the blend are not due to large-scale thermodynamic phase separation, but is imposed by the crystallization process.

4. Conclusions

We show that the changes in processing parameter have a large effect on the crystallization behavior; e.g. shear and thermal history of the polymer significantly accelerate the crystallization rate. We have demonstrated that lactam (monomer) acts as a plasticizer in inhibiting the crystal growth and thus plays a role opposite to that of nucleating agents which accelerate the crystallization kinetics. Comonomers have far greater effect than blends on the retardation of the crystallization kinetics. Comonomers decrease the rate of crystallization, whereas blending with amorphous nylon retards or accelerates the crystallization depending on the temperature crystallization in relation to the T_g of the amorphous nylon. Amorphous nylon appears to reside outside the lamellar stacks.

Acknowledgments

The authors would like to thank R. Williams and M. McDonnell for discussions, and I. Lazic, E. Uyehora and J. Belles for providing some of the characterization data. The authors acknowledge the financial support of this work by a grant from NSF (DMR 0098104).

References

[1] Kohan MI, editor. Nylon plastics handbook. New York: Hanser; 1995.
[2] Bottenbruchand L, Binsack R, editors. Technische thermplaste polyamide. Kunstoff handbuch, Munich: Hanser; 1998.
[3] Hinrichsen G, Lux F. Polym Bull 1990;24:79–86.
[4] Magill JH. Polymer 1962;3:655–64.
[5] Ramesh C, Keller A, Eltink S. Polymer 1994;35:2483.
[6] Wang Z-G, Hsiao BS, Murthy NS. J Appl Cryst 2000;33:690.
[7] Strobl GR, Schneider M. J Polym Sci, Polym Phys 1980;18:1343.
[8] Hsiao BS, Verma RK. J Synchrotron Radiat 1998;5:23.
[9] Verma RK, Marand H, Hsiao BS. Macromolecules 1996;29:7767.
[10] Hsiao BS, Wang ZG, Yeh FJ, Gao Y, Sheth K. Polymer 1999;40:3515.
[11] Murthy NS, Stamm M, Sibilia JP, Krimm S. Macromolecules 1989;22:1261.
[12] Murthy NS. Int J Polym Mater 2001;50:429.
[13] Murthy NS, Barton Jr. R. In: Chung FH, Smith DK, editors. XRD in polymer industry: industrial applications of X-ray diffraction. New York: Marcel Dekker; 2000. p. 495. Chapter 19.
[14] Wang W, Schultz JM, Hsiao BS. J Macromol Sci, Phys 1998;B37(5):667.
[15] Wang Z-G, Hsiao BS, Sauer BB, Kampert WG. Polymer 1999;40:4615.
[16] Hsiao BS, Wang Z-G, Yeh F, Gao Y, Sheth KC. Polymer 1999;40:3515.
[17] Ran S, Cruz S, Zong X, Fang D, Chu B, Hsiao BS, Ross R, Chang H, Londono D. Adv X-ray Anal 2000;43:344.
[18] Hoffman JD, Davis GT, Lauritzen Jr. JI. Treatise in solid state chemistry. New York: Plenum Press; 1976. Chapter 7; p. 497.
[19] Wunderlich B, Macromolecular physics, vol. 3. New York: Academic Press; 1980. p. 73.
[20] Lauritzen Jr. JI, Hoffman JD. J Appl Phys 1973;44:4340.
[21] Khanna YP, Murthy NS, Kuhn WP, Day ED. Polym Engng Sci 1999;39:2222.
[22] Ellis TS. Polymer 1998;29:2015.
[23] Ellis TS. Polymer 1990;31:1058.
[24] Ellis TS. Polym Commun 1991;32:489.
[25] Ellis TS. Polymer 1995;36:3919.
[26] Liu Y, Donovan JA. Polymer 1995;36:4797.
[27] Myers ME, Wims AM, Ellis TS, Barnes J. Macromolecules 1990;23:2807.
[28] Turnbull D, Fischer JC. J Chem Phys 1949;17:71.